Received: 31 May 2024 | Revised: 26 September 2024 | Accepted: 1 October 2024

DOI: 10.1002/suco.202400717

ARTICLE

fib CEB-FIP WILEY

Reliability and partial factor-based assessment of a highway bridge supported by nondestructive testing

Stefan Küttenbaum[1] | **Thomas Braml**[1] | **Marco Heinze**[2] | **Christian Kainz**[1] | **Christian Stettner**[2] | **Alexander Taffe**[3]

[1]Department of Structural Engineering, Universität der Bundeswehr München, Neubiberg, Germany

[2]ZM-I München GmbH, Munich, Germany

[3]Department 2: Engineering – Technology and Life, HTW Berlin – University of Applied Sciences, Berlin, Germany

Correspondence
Stefan Küttenbaum, Department of Structural Engineering, Universität der Bundeswehr München, Werner-Heisenberg-Weg 39, Neubiberg 85577, Germany.
Email: stefan.kuettenbaum@unibw.de

Funding information
Bundesministerium für Wirtschaft und Klimaschutz

Abstract

The preservation of the degrading transport infrastructure is vital, as replacing it is impossible in view of limited budgets and environmental impacts. One component in overcoming this challenge is the evaluation of the reliability and the calculation of the remaining service life of existing structures. These structural reliability reassessments allow for the identification and utilization of load-bearing capacity reserves. The consideration of actual structural characteristics and environmental conditions, various of which can be gathered by means of numerous measurement and inspection techniques, has the potential for more realistic computation results and therefore more economic decisions about the operation as well as maintenance activities. This article attempts to shed light on the potential of nondestructive testing (NDT) methods for updating the input variables in the ultimate limit states during a recalculation. The approach of the NDT-supported reliability reassessment is demonstrated using a prestressed concrete bridge emphasizing the bending proof in transversal direction. As a result, the semi-probabilistic, probabilistic and NDT-based reassessment results are compared and the effects of NDT-supported structural analysis on the calculated reliability are highlighted.

KEYWORDS

concrete bridge, existing structures, NDT, probabilistic methods, reliability assessment

1 | INTRODUCTION

The transport infrastructure is exposed to conditions that have fundamentally changed compared to the design and construction dates. Most of the structures have been in operation for a number of decades. The majority of the road bridges in Germany, for example, was built in the 1960s and 1970s. These have to withstand a significantly higher traffic volume than at the time of construction. Against the background of degradation and increasing requirements, the reliability assessment of existing structures such as bridges, tunnels, or retaining walls, many of which were raised according to outdated numerical and structural design rules, serves to evaluate their remaining service life and load-bearing capacity reserves. Therefore, efficient and realistic reassessment processes and results are an integral part of a preservation strategy striving for a safe, future-proof, economical, and sustainable infrastructure network.

The road bridge stock in Germany comprises 40,000 motorway and highway bridges. More than 25% were assigned a condition rating that is no longer satisfactory.[1] To compare the actual and the demanded load capacity,

the load index has been introduced. Noticeable shortfalls of the target load level are indicated for around 15%, measured by a load index larger than III.[2] The recalculation guideline[3,4] was introduced to provide a framework for the assessment of the actual reliability of those existing bridges considering recent traffic forecasts. Besides the mathematical reliability analysis itself, the condition assessment based on structural inspections according to the standard DIN 1076[5] and, if necessary, further in-depth investigations is part of the bridge reassessment program invented by the highway authorities.

The recalculation of a number of bridges has revealed the necessity to adapt the calculation models according to the Eurocodes for the economical application to existing structures.[6] Frequently observed numerical deficiencies were identified, clustered and the research work focused on them. Well-known examples are the area of the shear force capacity assessment of prestressed concrete structures with a low shear force reinforcement density, and the evaluation of the constructive design of reinforcement in existing structures[7–10] The on-site examination of the structures with regard to, e.g., mechanical and geometrical parameters forms another essential basis for the recalculation. The combination of these two disciplines, i.e., the structural inspection-supported reliability reassessment, has the potential to avoid premature interventions or extend the remaining service life of structures, as deeper knowledge about the considered system is the foundation for the justified utilization of load-bearing capacity reserves.

The aim of this article is to demonstrate the method, advantages, and limitations of supporting the reliability assessment of an existing structure through nondestructive testing (NDT) on-site. A prestressed concrete bridge with a t-beam cross section serves as case study. Both, semi-probabilistic and probabilistic analyses are carried out according to the Eurocodes. The focus is on the bending proof in transversal direction. Selected measurement results about the transversal tendons obtained using the ultrasound echo technique and the ground penetrating radar (GPR) method are incorporated. The values of the reliability calculated with these different levels of approximation are presented and compared. Parameter studies show, which effects on the numerical reliability could be achieved by bridge inspections.

Section 2 contains (a) the description of the applied procedure for NDT-supported reliability assessment, (b) the definition of the limit state equation, and (c) an overview of which input variables in the ultimate limit state (ULS) can be physically measured using the state-of-the-art NDT methods. Chapter 3 deals with the case study. The description of the prestressed concrete bridge is followed by the semi-probabilistic and probabilistic reassessment including sensitivity analyses and parameter studies in Section 3.2. The NDT results are analyzed and utilized in Section 3.3. The assessment results are summarized and discussed in Section 3.4.

2 | METHODOLOGY

The method reaching from the purposeful definition of on-site testing tasks to the reliability analysis under consideration of quality-evaluated inspection results will be outlined in Section 2.1. The limit state function in Section 2.2 serves as the basis for both (a) the matrix of non-destructively measurable basic variables for verifications in the ULS bending in Section 2.3 as well as (b) the reliability analysis of the investigated bridge in chapter 3.

2.1 | NDT-supported reliability assessment of existing bridges

Various destructive and NDT methods have been successfully applied to examine structural or environmental characteristics of concrete structures[11–13] These methods allow to collect data that describe such physical information *always* with an uncertainty. There is no doubt that such information must be true (in the sense of unbiased), both from an engineering and metrological point of view. However, it is not always necessary to determine physical properties with the highest achievable precision. Therefore, reasonable requirements should be set for (a) what should be measured, (b) how accurately, and (c) when and where. Their comparison with the capabilities of physically suitable inspection techniques then allows for the definition of testing tasks and subsequently for the development of efficient on-site inspection strategies or procedures,[14] respectively. This objective is pursued in the present research work on the one hand by semiprobabilistic and probabilistic structural reliability analyses (determining the demands) and on the other hand by inspection and measurement uncertainty considerations (expressing the capability of inspection techniques). Once a measurement strategy has been defined, the on-site inspections can be carried out and analyzed to incorporate the individually measured and quality-assured information into the structural reliability analysis by means of adjusted characteristic values and partial (safety) factors or updated stochastic models of the basic variables. The applied methodology[15,16] can be summarized as follows:

2.1.1 | Determination of testing tasks and development of inspection procedures

The initial structural reliability analysis of an existing structure (based on the information available prior to any testing) is performed. The relevance of information and

the requirements are derived through a combination of (a) engineering judgments, (b) semi-probabilistic recalculations to derive degrees of utilization, and (c) probabilistic analyses using the first- and second-order reliability methods (FORM, SORM) to compute values of the reliability index β[17–19] and to perform sensitivity analyses. The results of local sensitivity analyses, e.g., values of the sensitivity coefficient $\alpha_{\tau,i}$, indicate how strongly a basic variable influences the calculation result, i. e. the structural reliability, or how significantly a small change in a distribution parameter affects it. Additional parametric studies provide insights into the effects of a larger deviation between assumed and actual characteristics. They also allow for the definition of inspection requirements, such as maximum permissible measurement uncertainties.[15] The relevance and requirements are compared with the expected capabilities of the inspection techniques to set up suitable inspection procedures.

2.1.2 | On-site data acquisition and data analysis

The inspection procedure contains the information needed to reproducibly apply an inspection technique to a specific testing scenario, i.e., the scope (testing object, boundary conditions), the inspection objective, the extent (area, sample size, frequency), personnel requirements, system specifications, as well as information on the equipment settings, the data acquisition (e.g., resolution), data analysis (e.g., signal processing steps) and documentation.[20] This inspection procedure guides the testing personnel through the on-site data acquisition and subsequent data analysis. The NDT data evaluation, e.g., when applying the ultrasound-echo technique or ground penetrating radar (GPR), should be based on probability of detection (POD) analyses and measurement uncertainty considerations in order to answer whether one can reliably detect the object being searched for, and if so, how accurately.[21,22] The measurement uncertainty calculation can be performed according to the Guide to the Expression of Uncertainty in Measurement (GUM).[23–25] The outcome for quantitative testing tasks is a measurement result which at least consists of a best estimate $\hat{y}$, the attributed measurement uncertainty $u(\hat{y})$ expressed as standard deviation, and the distribution type of the measurand.

2.1.3 | Utilization of measuring results in reliability analysis

This third step aims to process the quality-assured measurement result into a stochastic model (basic variable) or further into a characteristic value and a modified partial factor, respectively, so that the measured information can be utilized in probabilistic and/or semi-probabilistic reliability assessment. When modeling basic variables, the fundamental challenges in the modeling process must be addressed and all relevant types of uncertainties covered.[26,27] These include the intrinsic, statistical, model, and measurement uncertainty[28,29] whereby the latter quantifies the precision of measured information. Details about the treatment of inspection uncertainties can be found in Section 3.3.1. From such a stochastic model of a basic variable, the characteristic value of the property can be derived as a quantile value and the partial factor modified.[16]

2.2 | Limit state function

The limit state function[30–32] to assess the bridge in Section 3 regarding ULS bending is.

$$g_{\mathrm{M}}(\boldsymbol{x}) = \theta_{\mathrm{R,M}} \cdot \left[\left(A_{\mathrm{s1}} f_{\mathrm{y}} + A_{\mathrm{p}} f_{\mathrm{p}} + \theta_{\mathrm{E,N}} \cdot \sum N_i \right) \cdot \left(d_r - \frac{k_{\mathrm{a}}}{\alpha_{\mathrm{R}}} \cdot \frac{A_{\mathrm{s1}} f_{\mathrm{y}} + A_{\mathrm{p}} f_{\mathrm{p}} + \theta_{\mathrm{E,N}} \cdot \sum N_i}{b \cdot \alpha_{\mathrm{cc}} \cdot f_{\mathrm{c}}} \right) - \theta_{\mathrm{E,N}} \cdot \sum N_i \cdot z_{\mathrm{sr}} \right] - \theta_{\mathrm{E,M}} \cdot \sum M_i - \theta_{\mathrm{E,N}} \cdot \sum N_i \cdot z_{\mathrm{sr}}$$

$$\text{with} \sum N_i = N_{\mathrm{G}} + N_{\mathrm{CS}} + N_T + N_{\mathrm{Q}} + N_{\mathrm{p,ind}}$$

$$\text{and} \sum M_i = M_{\mathrm{G}} + M_{\mathrm{CS}} + M_T + M_{\mathrm{Q}} + M_{\mathrm{p,ind}} \quad (1)$$

The description of the respective input quantities can be found in Table 1. In addition to the usual assumptions, the following definitions apply to this Equation (1):

- The concrete compression at the edge fiber reaches the limit strain: $\varepsilon_{\mathrm{cu2}} = 3.5‰$.
- The rebars and prestressing steel (with bond in this case) reach the theoretical yield strength: $\varepsilon_{\mathrm{s1}} \geq \varepsilon_{\mathrm{sy}}; \varepsilon_p \geq \varepsilon_{\mathrm{py}}$.
- The coefficients k_{a} and α_{R} in the parabolic-rectangular stress diagram are constant values.
- In case of statically indetermined systems, the determined part of the prestressing force is implicitly considered as resistance (multiplication of tensile strength f_{p} and cross-sectional area A_{p}); the statically indetermined part is explicitly considered as an action. In this (statically determined) study, the variables $N_{\mathrm{p,ind}}$ and $M_{\mathrm{p,ind}}$ are not applicable.

TABLE 1 Matrix of basic variables in ULS bending with indication of nondestructive measurability (+: Suitability proven in practical application; o: Associated indirect method; −: Physically not directly applicable).

Testing method / Basic variable		Ground penetrating radar (RA)	Impact-echo (IE)	Laser-induced breakdown spectroscopy (LIBS)	Magento-inductive methods (MI)	Potential mapping	Rebound hammer (RH)	Ultrasonics (US)	X-ray
$\theta_{R,M}$	Model uncertainty (bending resistance)	−	−	−	−	−	−	−	−
$\theta_{E,N}$	Model uncertainty (effect of actions; normal forces)	−	−	−	−	−	−	−	−
$\theta_{E,M}$	Model uncertainty (effect of actions; bending moments)	−	−	−	−	−	−	−	−
A_{s1}	Cross-sectional area of tension reinforcement	−	−	−	+	−	−	−	+
f_y	Yield strength of reinforcement	−	−	−	−	−	−	−	−
A_p	Cross-sectional area of prestressing steel	−	−	−	−	−	−	−	+
f_p	Tensile strength of prestressing steel	−	−	−	−	−	−	−	−
d_r	Effective depth	+	−	−	+	−	−	+	o
k_a	Coefficient	−	−	−	−	−	−	−	−
α_R	Coefficient	−	−	−	−	−	−	−	−
b	Width of the section	−	+	−	−	−	−	+	−
α_{cc}	Coefficient considering long term/unfavorable effects on f_c	−	−	−	−	−	−	−	−
f_c	Concrete compression strength	−	−	−	−	−	+	o	−
z_{sr}	Distance section center/reference axis	+	−	−	+	−	−	+	o
N_G	Normal force (N) due to dead loads	−	−	−	−	−	−	−	−
N_{CS}	N due to creep + shrinkage	−	−	−	−	−	−	−	−
N_T	N due to temperature	−	−	−	−	−	−	−	−
N_Q	N due to traffic loads	−	−	−	−	−	−	−	−
$N_{p,ind}$	N due to prestressing (statically indetermined part)	−	−	−	−	−	−	−	−
M_i	Bending moments (M); indices analogous to normal forces (N)	−	−	−	−	−	−	−	−

2.3 | Potential of NDT in reliability assessment

Table 1 contains the description of the basic variables included in Equation (1) and outlines the physical capability of frequently applied on-site NDT techniques, most of which were recently considered in the German qualification standard DIN 4871[33]:

- The model uncertainties linked to the level of approximation of the applied resistance and load models cannot directly be updated using the aforementioned NDT techniques.
- The cross-sectional areas of steel can be accurately measured using radiographic methods. Additional information about steel deterioration can be gathered. The magneto-inductive techniques allow for a diameter estimation of near-surface steel rebars if the concrete cover is known. Accompanying radar scans can help to identify multiple closely mounted steel rebars in order to correct biases when inspecting magneto-inductively.
- Geometrical dimensions of the cross-section can be laser-scanned. The NDT-techniques can provide additional information about component thicknesses. The impact echo allows robust statements to be made. Smaller thicknesses can often be determined using radar. For thicker components and in densely reinforced areas, the ultrasound is usually more expedient. Both volume methods ultrasound and GPR further allow for the determination of inner geometrical dimensions. The gathered data may be used to update, e.g., inner lever arms (z_{sr}, etc.).
- The sole use of the rebound hammer is not permitted on many existing bridges due to the carbonation-induced concrete hardening. It can however be applied to identify weak points relatively. A combination of indirect methods such as the rebound hammer or ultrasound with compression tests of drill cores is conceivable to establish individual reference curves.
- Potential mapping is capable to detect areas subjected to active corrosion.
- LIBS is capable to analyze the chemical composition of components, such as drill cores, e.g., to identify pollutants or to determine chloride ingresses or carbonation depths.

Information about various further inspection techniques can be found in the literature[11,13,34] As the technical capability of the testing methods depends on boundary conditions such as surface conditions, chemical compositions, material properties or geometrical dimensions, their suitability must always be assessed individually.

3 | PILOT STUDY

The road bridge will be introduced in Section 3.1. The partial factor and reliability-based assessment is provided in Section 3.2, where sensitivity analyses reveal the impact of structural inspections on the reliability. An example for the incorporation of NDT data can be found in Section 3.3.

3.1 | The investigated prestressed concrete bridge

During the project launch, emphasis was placed on incorporating different concrete bridges that are typical for the road bridge stock in Germany.[35] This article deals with a prestressed single-span concrete bridge built in the 1970s. A view is given in Figure 1. The 38.45 m long superstructure carries a two-lane federal highway at an oblique angle over a river. No significant damages affecting the structural safety have been observed during the recurring inspections.

The cross-section was designed as t-beam with two main girders, cantilever arms on both sides, and a haunched deck slab, as shown in Figure 2. The superstructure is prestressed in longitudinal and transversal direction. The longitudinal beams are rigidly connected in the support axes through longitudinally prestressed cross beams.

Considering its slenderness and overhang, the focus of the reassessment was placed on the transversely prestressed slab, as the increased traffic loads have a greater effect on the reliability of the slab than on the reliability of the main girders. Against the background that the utility of NDT in the context of reliability reassessments is to be analyzed, another reason is, that deviations in the position of reinforcing and prestressing steel have greater impacts on reliability in reassessment of *thinner* components.

3.2 | Reliability reassessment without NDT results

3.2.1 | Semi-probabilistic reassessment—Modeling

The guideline-compliant definition of the *target load level* is based on the average daily heavy vehicle occurrence ("DTV-SV"), the number of lanes, and the traffic type. Although less than 2000 heavy vehicles, which is defined as threshold, have been observed in traffic counts, the target load model "BK60/30" for long-distance traffic according to the recalculation guideline and DIN 1072[36]

FIGURE 1 Lateral view of the investigated bridge.

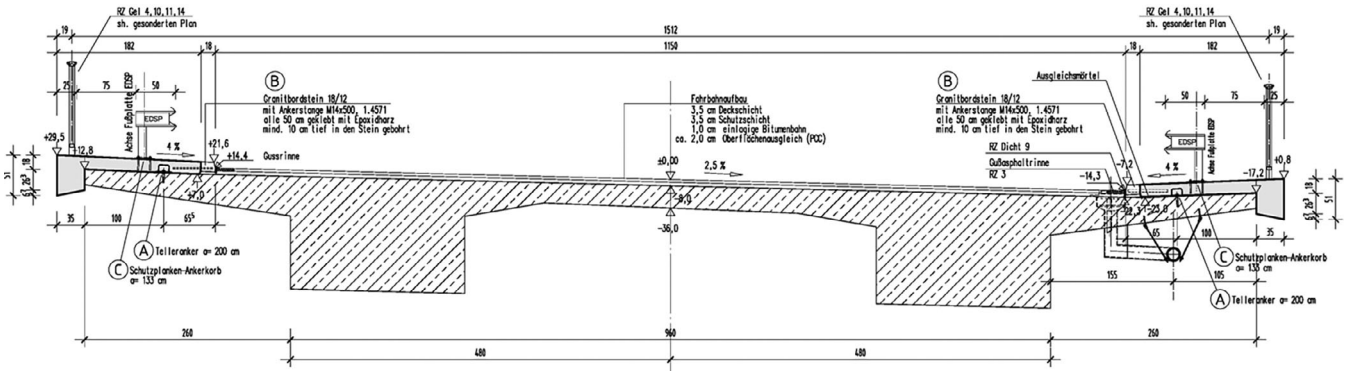

FIGURE 2 Cross-section of the investigated bridge indicating the transversal prestressing.

has been raised to load model 1 (LM 1) according to DIN FB 101,[37] as the carried highway serves as an important detour route. While the applied LM 1 is conceptually consistent with the Eurocode 1, BK60/30 would be based on the assumption of a 60 t and a 30 t vehicle on the main and secondary lane in addition to distributed loads.

As *computation model*, the northern main structure can be statically described as a single-span girder. The double-webbed girder is hinged on the supports, whereby the girder is statically determinate. The load-bearing behavior of the structure is mapped in the main load-bearing direction with beam elements. For the load distribution in the transverse direction, plate elements are defined for the superstructure, which only distribute the acting loads in transversal direction. The superstructure is articulated mounted. On the side of the southern support axis, the t-beam is supported with longitudinal displacement. The supports are fixed in the northern support axis and were generated using spring elements (Figure 3). The coupling to the superstructure takes place in the nodes of the respective support axis. The coupling conditions are defined according to the support scheme. Figure 4 shows an example of the defined restraints and coupling of the superstructure to the supports for the northern axis.

3.2.2 | Reinforcement

The longitudinal reinforcement is modeled as reinforcement line according to its vertical position. Individual reinforcement points are defined at the outer edges of the reinforcement lines for the program-internal definition of the t-beam. For the calculation of the required

FIGURE 3 Computation model.

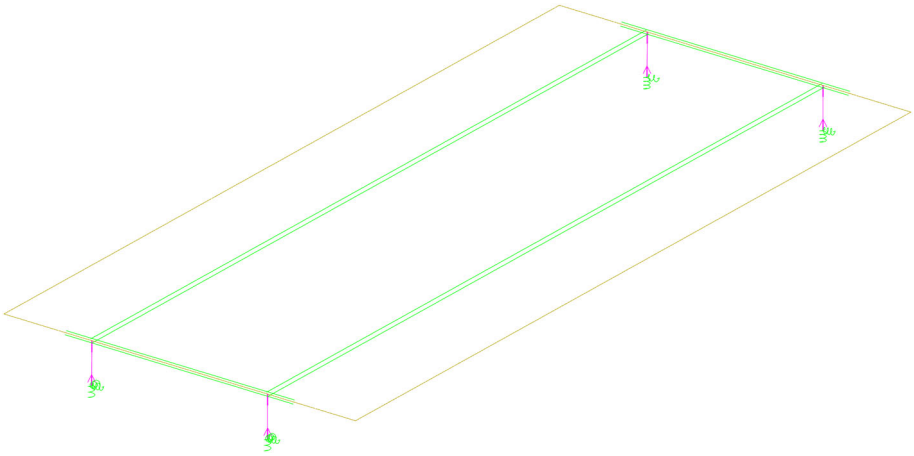

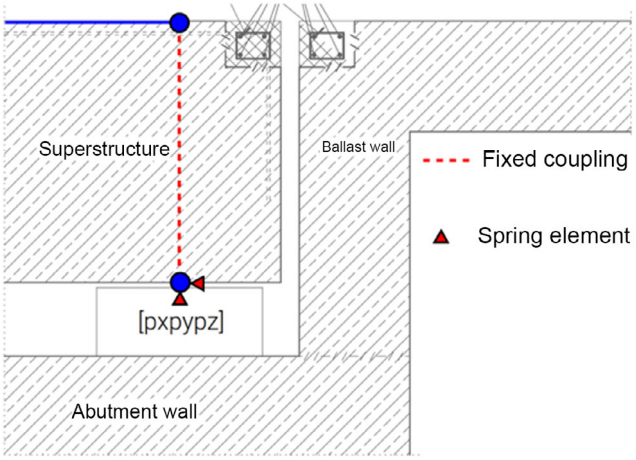

FIGURE 4 Coupling support area—northern bearing axis.

longitudinal torsional reinforcement, a reinforcement point is arranged in the corners within the web.

The longitudinal reinforcement plotted in Figure 5 is ribbed steel of grade St 420. In the transversal direction, ribbed St 420 steel has been mounted (see Figure 6) as reinforcement in addition to the tendons. The as-planned concrete cover is 3.0 cm. Due to the skew angle of the superstructure, additional reinforcement is arranged in the corner areas. The stirrup reinforcement was designed as a two-part stirrup. The overlap is at the height of the horizontal legs (see Figure 7).

3.2.3 | Prestressing

The superstructure is prestressed both longitudinally and transversely. Each web contains 33 tendons in longitudinal direction as plotted in Figure 8. The slab has been transversely prestressed with 123 tendons reaching across the entire width. The tendon length decreases to both sides towards the abutments due to the skewness (see Figure 9). According to the drawings, the alternately tensioned strands are mounted at a distance of 0.33 m. Tensioning was carried out on a reduced slab cross-section. The slab width was shortened by a total of 16 cm. After applying the prestressing, the remaining cross-section has been reinforced and concreted. The tendons are anchored at a distance of approx. 0.44 m from the reduced slab edge (see Figure 10).

3.2.4 | Semi-probabilistic reassessment—Bending in the transversal direction

The cross-sections decisive in the reassessment are determined based on the geometry, on the material parameters, as well as on the internal forces and moments. The partial (safety) factors used for permanent and moving loads are $\gamma_G = 1.35$ and $\gamma_Q = 1.50$. On the resistance side, the reinforcing and prestressing steel layers were constructed evenly in longitudinal direction, so that no major jumps in the cross-section load-bearing capacity are to be expected. The four crucial sections depicted in Figure 11 have been investigated according to DIN FB 102[38] in the ULS.

The rigidity loss during the transition to state II is taken into account by reducing the constrained internal forces due to temperature stresses by the factor $f(EI^I/EI^{II}) = 0.6$ in accordance with DIN FB 102:2009, Section 2.3.2.2. The decisive design internal forces result from the application of the live load as a leading action. For this reason, the actions due to temperature are multiplied by the following factor (Equation 2).

$$f\left(EI^I/EI^{II}\right) \cdot \gamma_E \cdot \psi_1 = 0.60 \cdot 1.35 \cdot 0.80 = 0.65 \qquad (2)$$

The verification is based on the relative load-bearing capacity between the numerical and the ultimate moment. Under consideration of the reinforcement, the load-bearing capacity is verified in a first step using

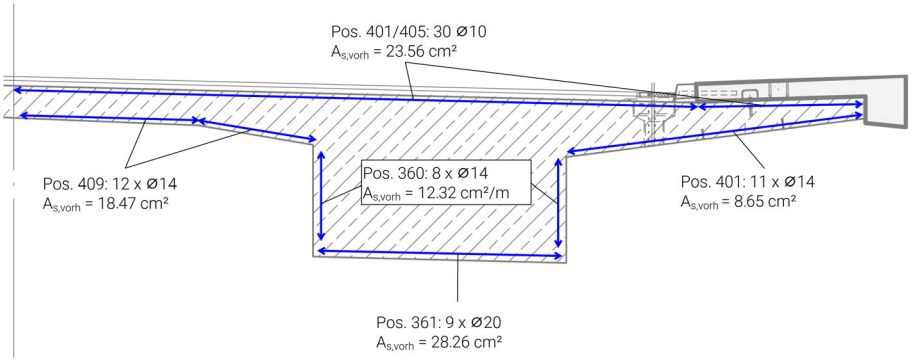

FIGURE 5 Existing longitudinal reinforcement–section bridge axis/t-beam; $A_{s,vorh}$—planned cross-sectional steel area.

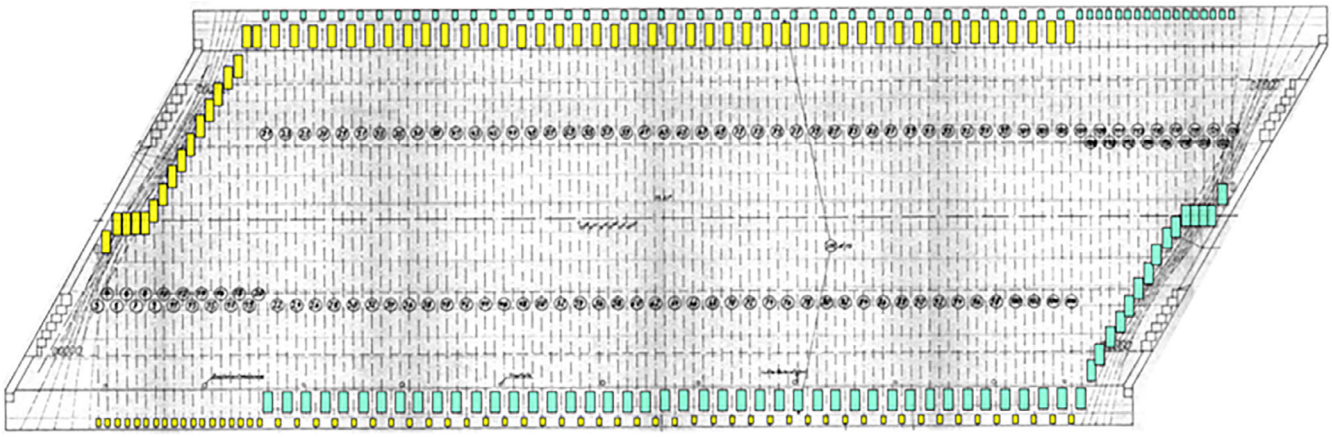

FIGURE 6 Existing transversal reinforcement–section bridge axis/t-beam.

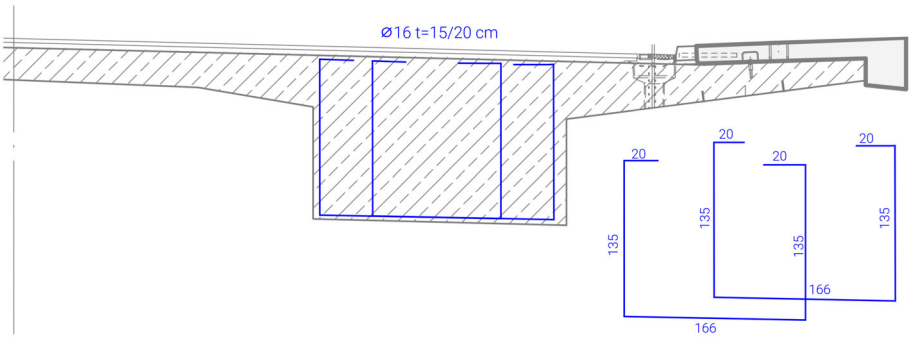

FIGURE 7 Existing stirrups—web of the t-beam.

the prestressing force increase of the tendons. The results using the positive or negative moments are given in Figures 12 and 13. The values show sufficient load-bearing capacity for the decisive sections in the transverse direction. The maximum capacity utilization has been obtained for the slab in the middle of the span (positive bending moment).

3.2.5 | Probabilistic reassessment

For the (full-) probabilistic assessment, the FORM as well as the SORM and the commercial software *STRUREL*[39] were used. The probabilistic assessment is presented for the slab section S3, which exhibits a high capacity-to-demand ratio and a good accessibility for the subsequent inspections; see Figure 11.

In the developed workflow, the internal forces computed with the aforementioned finite element model must first be transformed in order to utilize them as stochastic models in probabilistic analysis. The semi-probabilistic proof yields characteristic values X_k. In contrast, the distribution functions used as basis for probabilistic analyses are defined by expected values and variation parameters. The transformation of the characteristic values X_k to the mean values μ_x can be based on

the multiplication with conversion factors ζ,[40] see Equation (3).

$$\mu_x = \zeta \cdot X_k \tag{3}$$

Depending on the distribution type (frequently used types in structural reassessment are: Normal (N), Log.-normal (LN), and Gumbel), the conversion factors ζ can be calculated with Equations (4)–(6), where v is the coefficient of variation, $\Phi^{-1}(q)$ the quantile value, and γ the Euler's constant.

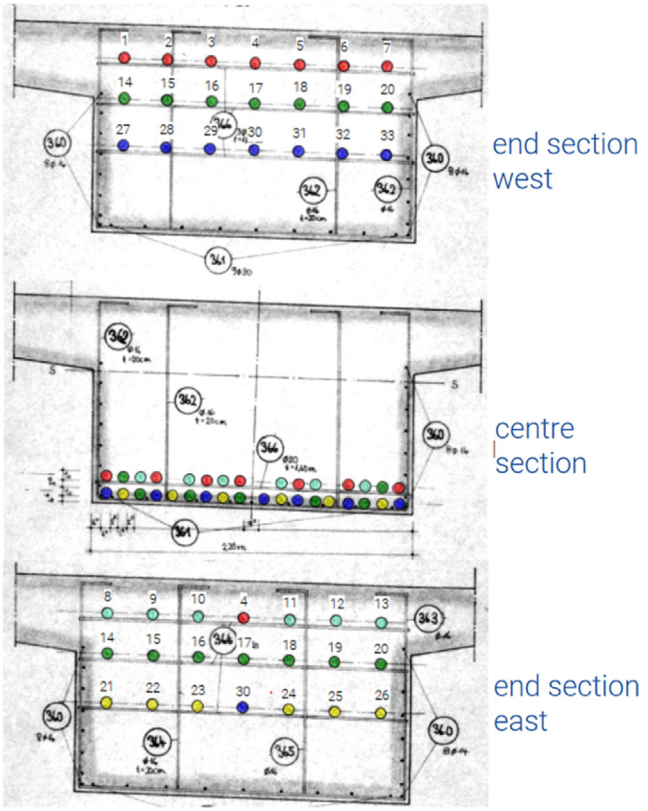

FIGURE 8 Longitudinal tendon arrangement.

$$\zeta_N = \frac{1}{(1 + v_x \cdot \Phi^{-1}(q))} \tag{4}$$

$$\zeta_{\mathrm{LN}} = \frac{1}{\exp[-0.5 \cdot v^2 + v \cdot \Phi^{-1}(q)]} \tag{5}$$

$$\zeta_{\mathrm{GUMBEL}} = \frac{1}{\left\{1 - v \cdot \frac{\sqrt{6}}{\pi} \cdot (\gamma + [\ln(-\ln q)])\right\}} \tag{6}$$

When converting characteristic values into extreme value distributions to characterize time-variant actions, the reference period must be in line with the target reliability (in this case $T = 50$ a). The characteristic values of the traffic loads correspond to 98% quantiles, i.e., to a return period of 50 years and a reference period of $T = 1$ a. The mean value $\mu_{T=50}$ can be observed from the mean value $\mu_{T=1}$, which was calculated beforehand using equation (6), through $\mu_{50} = \mu_1 \cdot \left(1 + \sqrt{6}/\pi \cdot v \cdot \ln(50)\right) = 1.46\mu_1$. Table 2 shows the input parameters describing the internal forces for the probabilistic calculation.

Table 3 contains the statistical parameters characterizing the structure. The model uncertainties ($U_{\mathrm{R,M}}$, $U_{\mathrm{E,M}}$, $U_{\mathrm{E,N}}$) are assumed to be log.-normally distributed (LN). The area of the longitudinal reinforcement a_{sl} ($Ø = 10$ mm, $s = 20$ cm, 3.93 cm^2/m) and the yield strength of the reinforcement ($f_{\mathrm{yk}} = 420$ N/mm^2) as well as the steel area of the tendons (Sager & Wörner Typ 31, $A_{\mathrm{p}} = 3.50$ cm^2, $s = 0.33$ m) and the yield strength of the tendons (St 145/160, $f_{\mathrm{pk}} = 1420$ N/mm^2) are modeled using a normal distribution. The height of the slab ($h = 45$ cm next to the inner web edge) and the distance between the tendons and the undersurface of the slab ($d_{\mathrm{sp}} = 24.5$ cm relative to the tendon axis according to the plans) are modeled with a normal distribution (N). The other geometrical parameters as well as the concrete compressive strength are represented by deterministic values due to their small influence on the load-bearing

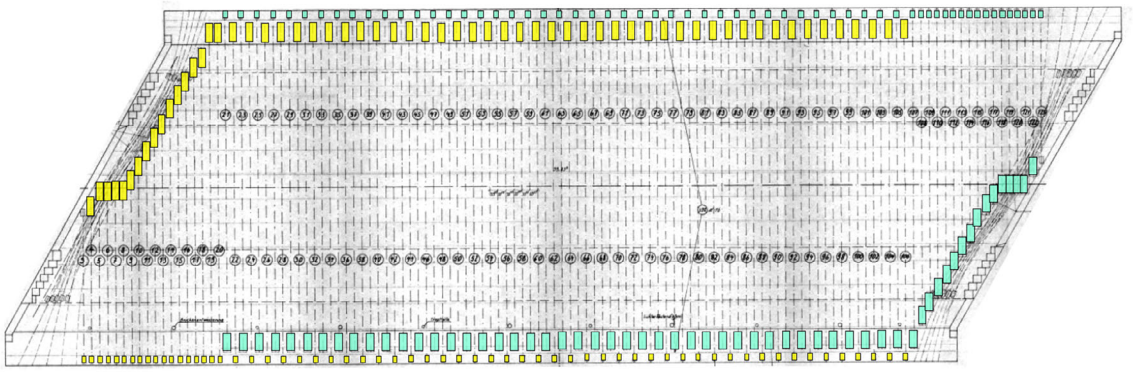

FIGURE 9 Transversal tendon arrangement (top view).

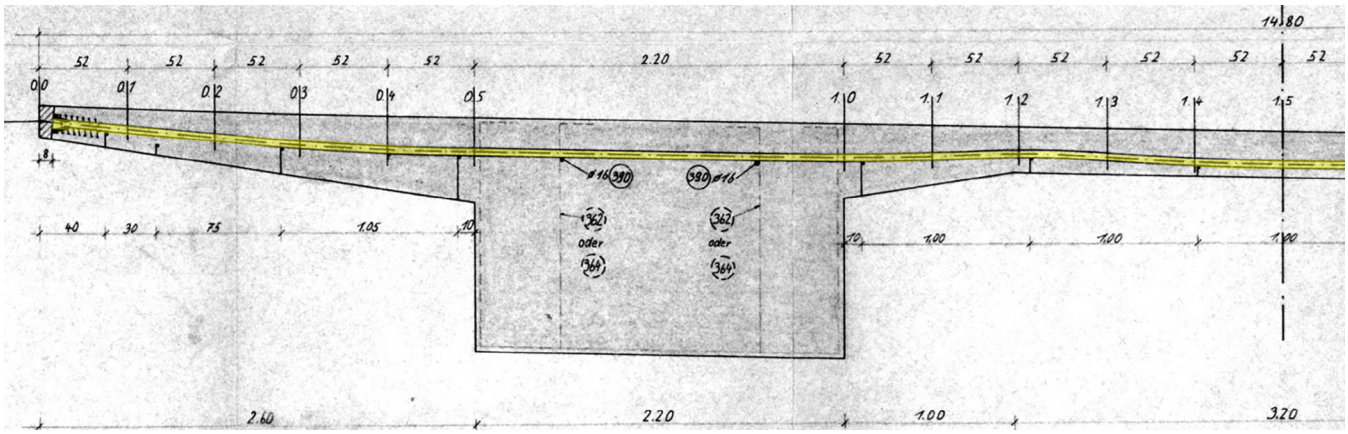

FIGURE 10 Transversal tendon course (cross-section, left side).

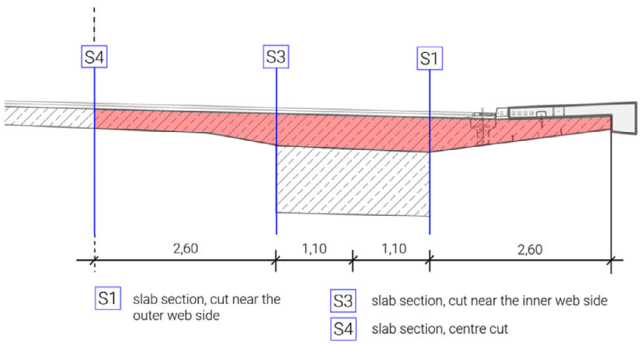

FIGURE 11 Definition of investigated sections for proofs in transversal direction.

capacity in this bending proof. However, it should be noted, that, e.g., the concrete strength underlies great variability and should thus not be modeled deterministically when conducting assessments in general.

The results of the full-probabilistic calculations show good alignment with the semi-probabilistic assessment. The solution of the FORM gives a reliability index of $\beta_{\mathrm{FORM}} = 6.90$ and the SORM results in a slightly smaller reliability index of $\beta_{\mathrm{SORM}} = 6.87$. The target reliability index according to DIN EN 1990 of $\beta_{\mathrm{target}} = 3.80$ for a reference period of 50 years and reliability class RC2 could thus be proven.

3.2.6 | Sensitivity analysis and parameter studies

A sensitivity analysis informs about the contribution of each parameter to the structural reliability. Figure 14 shows the values of the (geometrical) sensitivity factor α, describing the sensitivity of the reliability index against small changes in the mean of the standardized variable, for ULS bending according to Equation (1). Besides the model uncertainties $U = \theta$, the acting bending moments can be attributed significant relevance. The alpha value of the moment due to traffic loads M_{UDL} reveals the highest sensitivity. The geometrical position of the tendons d_{sp} and the material strengths of the rebars f_{y} and tendons f_{p} as well as the cross-sectional area of the tendons a_{p} also have a noteworthy sensitivity.

Based on the noticeable influence of the cross-section and position of the tendons, the influence of (larger) changes in the mean and the standard deviation of d_{sp} on the structural reliability has been analyzed (Figure 15). A value of $d_{\mathrm{sp}} = 24.5$ cm is stated in the drawings. Figure 15 shows the change of the reliability index β_{SORM} for a variation of the mean values μ_{dsp} on the left and for a variation of the standard deviation σ_{dsp} on the right. An increase in d_{sp} equals a higher vertical position of the tendons in this section, which is more favorable for the bending moment-bearing capacity against negative moments, because the internal lever arm increases. This effect can be observed in the parameter study, as the reliability index increases with an increased mean value μ_{dsp}. On the other hand, an increase in the standard deviation σ_{dsp} leads to a reduced reliability of the structure due to the higher associated uncertainty.

3.3 | Reliability assessment with NDT results

3.3.1 | On the treatment of inspection uncertainties

A measurement serves to determine the estimated value $\hat{y}$ of a measurand Y, which is assumed to approximate an unknown exact value. The uncertainty associated with this measured value $\hat{y}$ can be quantified by the combined

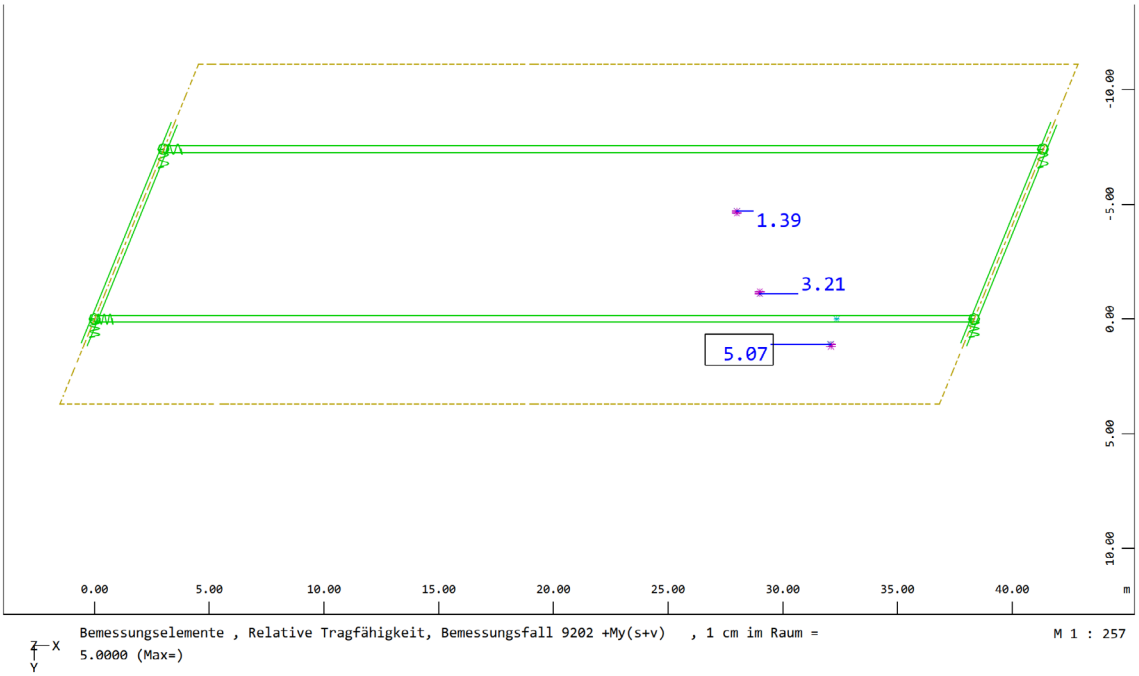

FIGURE 12 Relative load capacity—maximum bending moments.

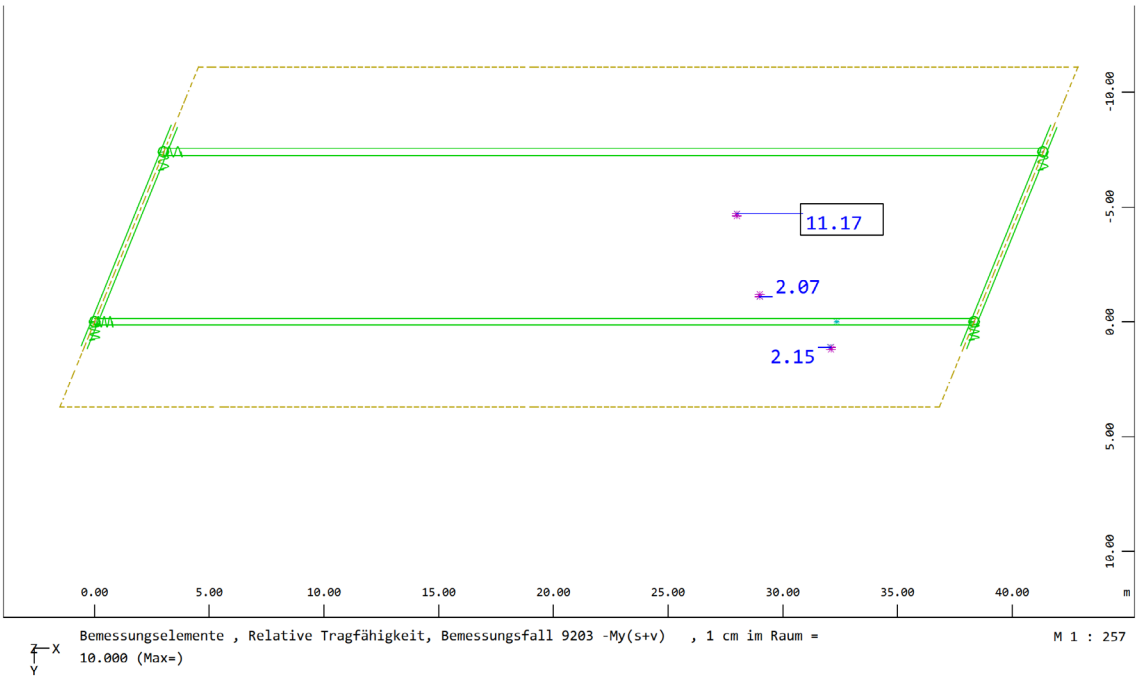

FIGURE 13 Relative load capacity—minimum bending moments.

standard measurement uncertainty $u(\hat{y})$, which expresses the measurement uncertainty as standard deviation. Measurement uncertainty (a) establishes confidence in measurements, such as quantitative structural inspections, (b) is inversely proportional to the precision (provided, that systematic errors have been corrected), and (c) indicates the quality of measured information. If information is used for decision-making, the reliability of the decision essentially depends on its quality.

The rules to calculate measurement uncertainty according to the Guide to the Expression of Uncertainty in Measurement (GUM) can be found in

TABLE 2 Statistical parameters of the internal forces for a bending failure at slab Section 3 (with TS – tandem system; UDL – uniformly distributed loads; N – Normal; GUM – Gumbel).

Component	Distribution type	Quantile q	CoV (–)	Factor ζ	$M_{y,50}$ (kNm/m)	$N_{y,50}$ (kN/m)
Dead weight G1	N	95%	0.06[41]	0.91	−36	21
Addit. dead load G2	N	95%	0.10[42]	0.86	−19	2
Creep/shrinkage CS	N	50%	0.30[43]	1.00	4	34
Temperature T_M	GUM	98%	0.15[44]	0.72	−1	0
Traffic load TS	GUM	98%	0.10[45]	0.794	−19	7
Traffic load UDL	GUM	98%	0.10[45]	0.794	−75	−91

TABLE 3 Mean value and coefficient of variation (CoV) for the structural basic variables at slab Section 3.

Component	Distribution type	CoV (–)	Mean value	Standard deviation
$U_{R,M} = \theta_{R,M}$ (–)	LN	0.07[46]	1.025	0.072
$U_{E,M} = \theta_{E,M}$ (–)	LN	0.10[30]	1.000	0.100
$U_{E,N} = \theta_{E,N}$ (–)	LN	0.05[30]	1.000	0.050
a_{s1} (m^2/m)	N	0.05	3.93×10^{-4}	2.0×10^{-5}
a_p (m^2/m)	N	0.05	1.06×10^{-3}	5.3×10^{-5}
f_y (MN/m^2)	N	0.067	450	30[47]
f_p (MN/m^2)	N	0.026	1536	40[48]
h (m)	N	0.02[30]	0.450	0.009
d_{sp} (m)	N	0.04	0.245	0.01[47]
b (m)	Const.	–	1.000	–
c_{nom} (m)	Const.	–	0.030	–
d_{St} (m)	Const.	–	0.014	–
k_a (–)	Const.	–	0.400	–
α_R (–)	Const.	–	1.000	–
α_{cc} (–)	Const.	–	0.850	–
f_c (MN/m^2)	Const.	–	30	–

JCGM 100:2008[49] and are summarized as flow chart in Figure 16. The key challenge is to develop an individual measurement model $Y = f(X_i)$ linking the measurand Y to a number of input quantities X_i known to be involved in the measuring process. The error propagation of these input quantities serves to calculate the measurement uncertainty. The investigation of the uncertainty contributions of the individual variables supports the appropriate selection of both an experimental design and a measurement model. The GUM procedure can also be applied to nondestructive concrete inspection.[50] Measurement models have already been developed for the testing tasks considered in this case study.[15,25,51] Due to the individual scope of application, it must be carefully assessed which components of existing models need to be updated if they are to be transferred to other inspection scenarios.

When incorporating measurement results into structural reliability analyses with probabilistic methods, the general issues in stochastic modeling of basic variables must be appreciated, e.g., the effects of competing models, the quantification of correlation, the tail-sensitivity problem, and the consideration of all relevant types of uncertainty.[26–29]

3.3.2 | On-site inspection results

On-site inspection

The exemplary measurement for utilization in reliability assessment is the position and mounting depth of the transversal prestressing strands in the bridge deck. This tasking can be solved, e.g., by ultrasonic-echo (UE) or ground penetrating radar (GPR) inspections, and intends to verify or reconstruct as-built drawings. The distance between the strands (lateral position) in longitudinal bridge direction and their depth related to the concrete

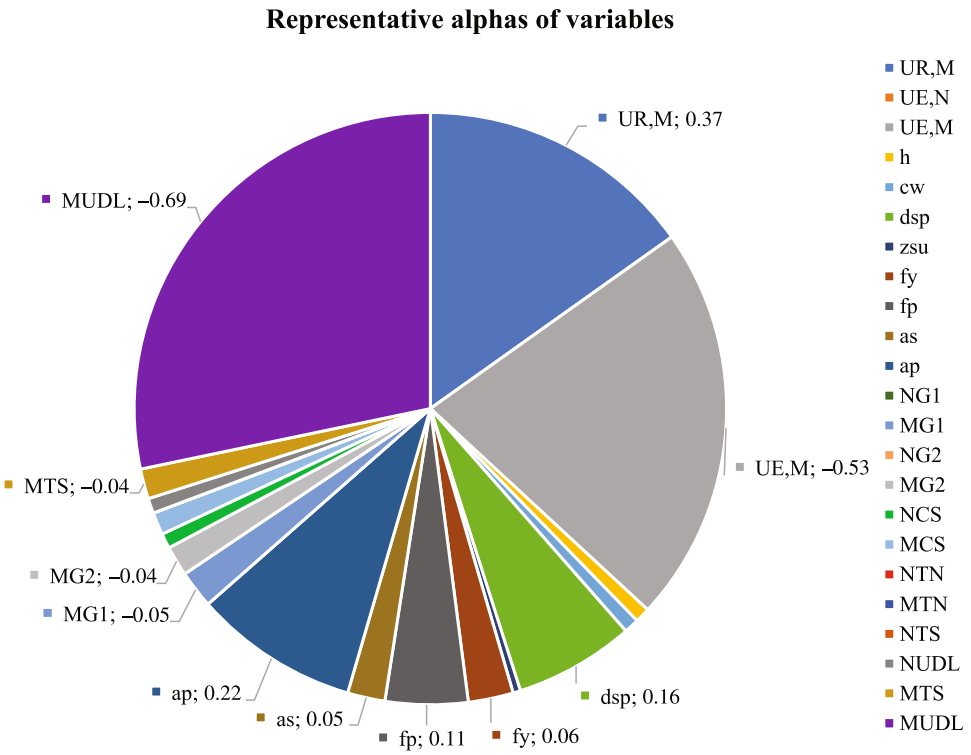

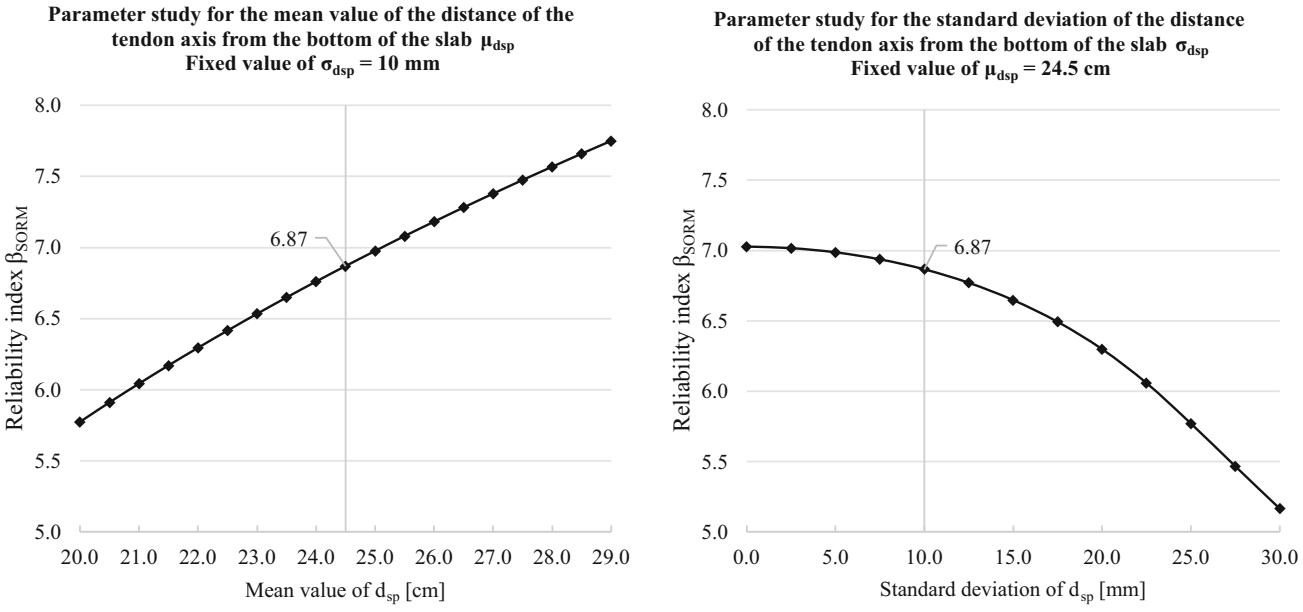

FIGURE 14 Sensitivity coefficients describing the influence of each input quantity (basic variable) on reliability.

FIGURE 15 Parameter study to predict the effects of changes in the distribution parameters of the vertical tendon position on the reliability index.

undersurface measured by GPR and UE have been statistically evaluated. The measurements considered in this section were performed along a line at the top of the beam in the section S3 (see Figure 11) through the bridge deck, as shown in Figure 17.

The radar inspection has been carried out with a step frequency antenna covering a range from 0.2 to 4.0 GHz. The B-Scan of 7.4 m length in Figure 18 shows reflections of near-surface rebars and the position of the transverse tendons. Each respective hyperbola apex is marked with a tag.

Ultrasonic echo was performed with an array of 48 cm aperture and a center frequency of approx. 40 kHz. The B-Scan in Figure 19 reveals the estimated positions

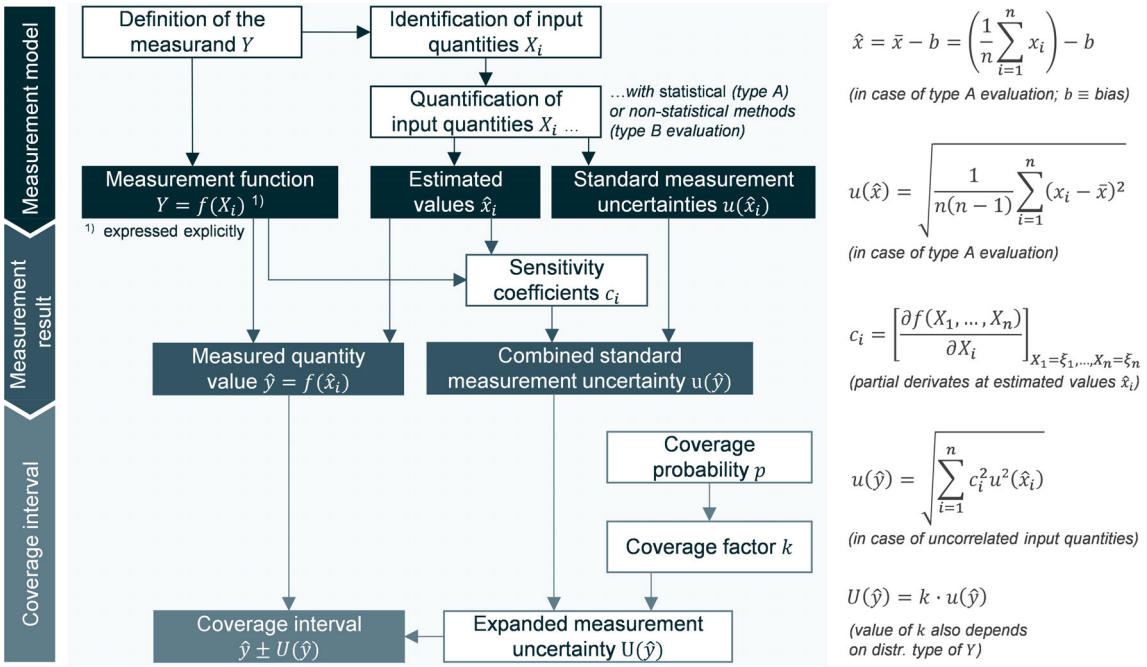

FIGURE 16 Calculation of measurement uncertainty according to JCGM 100:2008 for one normally distributed measurand.[51]

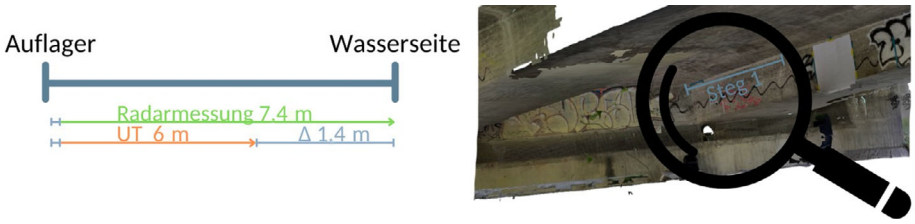

FIGURE 17 Position and length of the lines measured with radar and ultrasonic echo at the upper side of the beam vertically into the bridge deck.

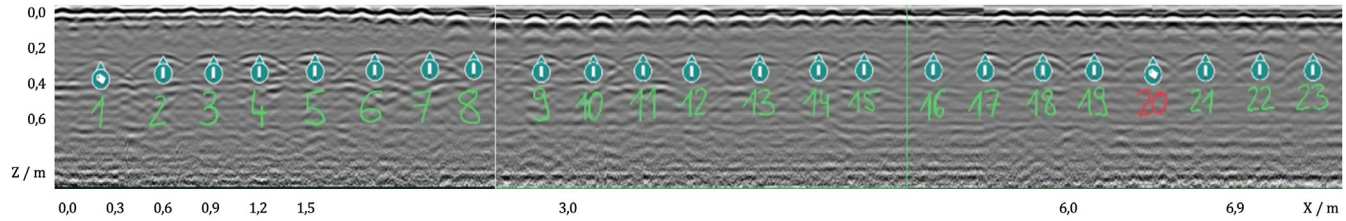

FIGURE 18 B-scan from Radar along 7.4 m with tags marking the position of the transverse tendon ducts.

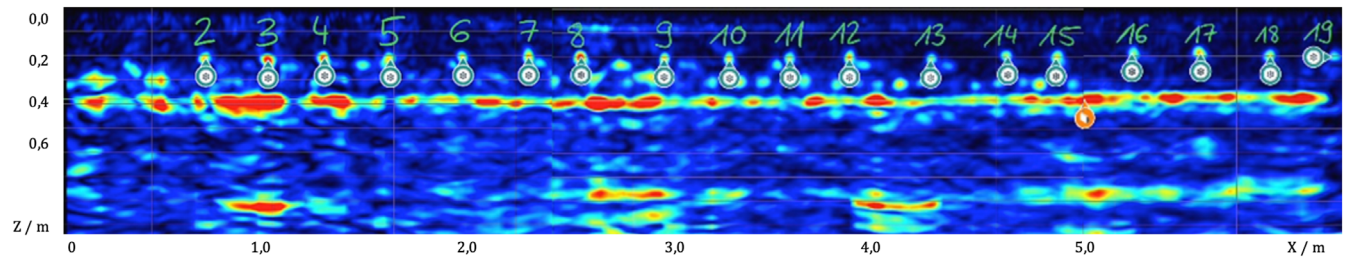

FIGURE 19 B-scan from ultrasonic echo along 6.0 m with tags giving the position of the transverse tendon ducts. The backwall can clearly be seen and is suitable for the estimation of the wave propagation velocity ($C_T = 2.757$ m/s).

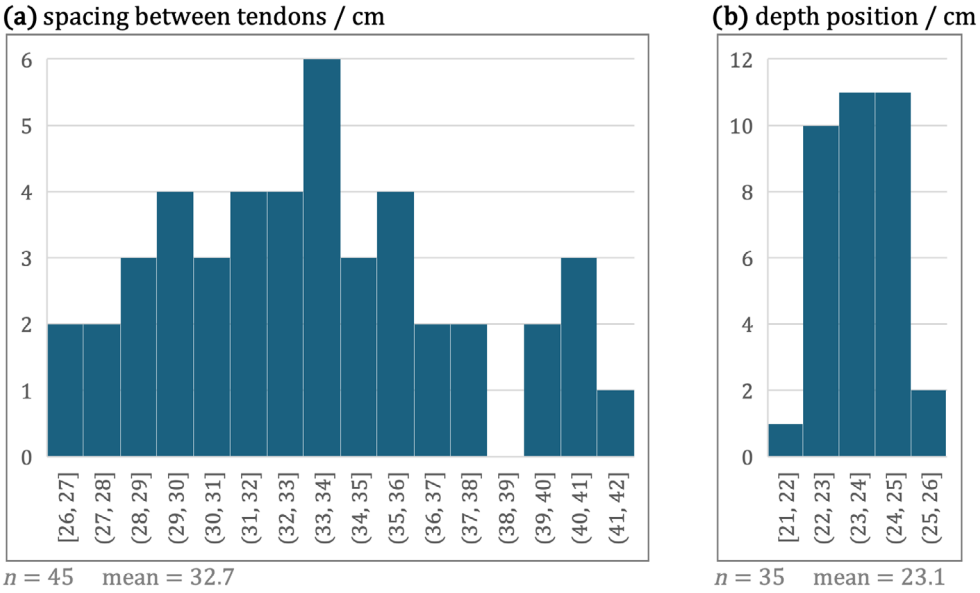

FIGURE 20 Picked values for (a) the spacing between transversal tendons and (b) the vertical position of the tendons related to the concrete undersurface/cm.

of the transverse tendon ducts (tagged). The backwall is clearly visible at a depth of approx. 44 cm, which relates to the thickness of the slab that has been read out from the as-built-drawings with 43.9 cm. Based on that thickness, the offset and the time of flight, the wave propagation velocity has been calculated with 2.757 m/s. As expected, radar does not reveal the backwall as clear as ultrasonic echo.

The tendons #2 to #19 were detected and localized with both methods. The spacing between the tendon duct axes varies between 23 and 41 cm. According to the as-built drawings, the spacing should be 33 cm. Comparing the estimated lateral positions between radar and ultrasound, it is in 6 of 18 cases the same value, in 10 cases less than 2 cm difference and in one case $\Delta \approx 4$ cm. In total, the estimation of the lateral position (not the relative spacing) is reliable within a range of approx. ± 1–2 cm in most cases. The depth range from ultrasonic echo varies between 22 and 25 cm. According to the as-built drawings, the depth should be 24.5 cm.

Statistical evaluation

The GPR data is used to determine the spacing between the transversal tendons and the gathered ultrasound data to compute the vertical position of the tendons exemplarily for section S3 according to Figure 11. Picking the respective volume elements yields the following dimensions:

The picked values of the depth position in Figure 20b were corrected by the radius $r = 1.06$ cm to express the distance between the *center* of the prestressing strand cross-section and the concrete undersurface $\bar{x} = 24.1$ cm. The identified systematic errors result from the offset, change in impulse shape, competing points in tendon reflections, and the spacing between transmitter and receiver.[51] They have been corrected prior to the measuring data reconstruction.[25]

The precision in depth position measurement using ultrasound has been quantified using existing models of the measurement.[15,51] These computations are delimited in this contribution. The measurement uncertainty achievable in previous and comparable inspection scenarios has been found to be approx. $u(\hat{y}) = 0.6...0.7$ cm.[15] The measurement result for the tendon position in this specific cross-section S3 is composed of the distribution type, the measured quantity value, and the standard measurement uncertainty: $Y \sim N(\mu = \hat{y} = 24.1\,\text{cm}; \sigma = u(\hat{y}) = 0.75\,\text{cm})$. The inspection thus allows for a slightly reduced uncertainty to be covered in reliability analysis and yields a mean value which is individually consistent with the information available prior to testing. It is conceivable to incorporate the observations made about further surrounding transversal tendons, as their curves are assumed to be identical both in the drawings and in the finite element model. This would lead to a slightly shifted mean and a reduced value of the standard measurement uncertainty, which then depends primarily on the number of considered tendons (Figure 21). The impact on structural reliability will be demonstrated in the following section.

The spacing of the transversal tendons can be associated with a comparably low measurement uncertainty as the *relative* distance between the reflections within one measuring dataset is the quantity of interest. Absolute specifications of dimensions are redundant. In-depth measurement uncertainty calculations have not been carried out to avoid an uneconomical assessment process, as uncertainties in the sub-millimeter range were

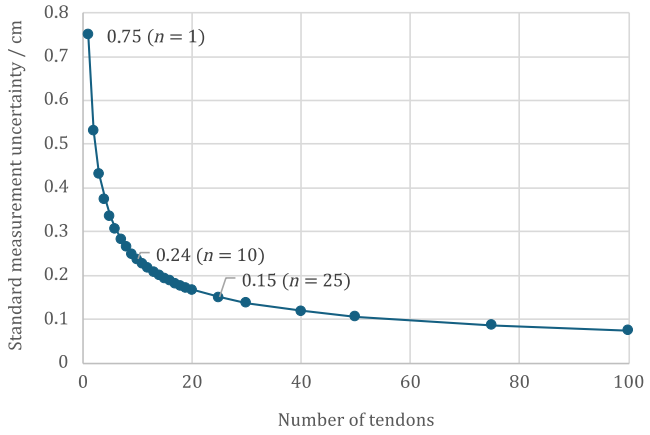

FIGURE 21 Standard measurement uncertainty against number of incorporated transversal tendons.

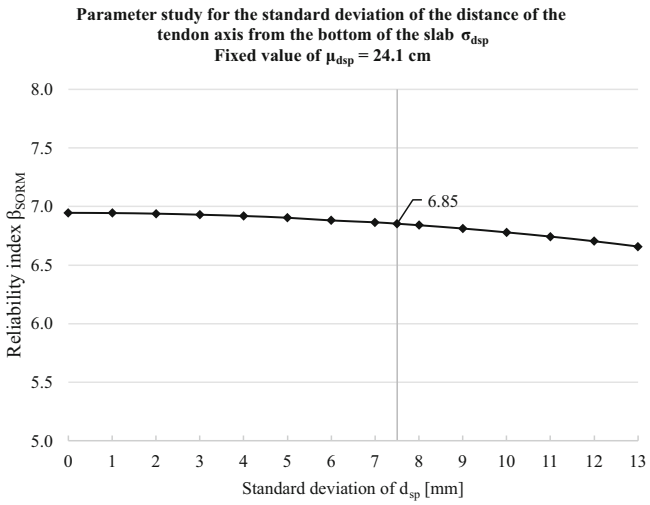

FIGURE 22 Parameter study for the standard deviation of the vertical position of the tendons with measured mean value.

expected.[25] Instead, the measured value is expressed deterministically for the purpose of use in structural reliability analysis. The mean spacing in the structurally analyzed section S3 can be given as 32.7 cm. This value is also in line with the information from the plans (33 cm). In cases where (a) reducing the uncertainty of this spacing to update the cross-sectional area of the prestressing steel A_p is beneficial, (b) a significant deviation from the assumed spacing has been measured, or (c) information is in doubt or not available, the use of the GPR is considered an economical and often reliable option for gathering information about the amount of rebars or tendons and their relative distance to each other.

3.3.3 | Updated reliability assessment using NDT results

Based on these NDT results, the probabilistic calculation can be repeated with adapted input parameters. In this study, the position of the tendons d_{sp} is updated. The measured mean value of $\mu_{dsp} = 24.1$ cm and a standard deviation of $\sigma_{dsp} = 7.5$ mm are considered. Due to the high consistency between as-built drawings and the inspection result, the updated reliability indices show close alignment with the initial probabilistic analysis in Section 3.2.3. Although the mean value μ_{dsp} indicates a slightly more unfavorable position of the tendons, overall, the updated reliability index β is slightly increased due to the uncertainty reduction in the standard deviation σ_{dsp}. The analysis based on NDT data gives a reliability index of $\beta_{FORM} = 6.88$ and $\beta_{SORM} = 6.85$.

Figure 22 shows an updated parameter study for the influence of the standard deviation on the reliability index appreciating the nondestructively measured mean value $\mu_{dsp} = 24.1$ cm in order to estimate the effects of considering a number $n > 1$ localized tendons on reliability. It may be mentioned that updating the reliability analysis is particularly useful, when information is missing or doubted, or when the utilization ratio is close to thresholds. A close alignment between drawings and inspection results can, however, be seen as confirmation of initial assumptions.

3.3.4 | Partial factor modification

(Full-) probabilistic calculations require expert knowledge and might lack in comparability. The modification of partial factors can enhance the semi-probabilistic degree of utilization and lead to a more economical computation by reducing uncertainties based on new information. Documents like the Bulletin 80,[52] Model Code 2020,[53] and DBV-booklet 24[54] provide procedures for these modifications ensuring that the modified factors align with the desired level of safety. The partial factors depend on the following parameters: Target reliability index β_{target}, distribution type of the respective basic variable X_i, fractile of the characteristic value, coefficient of variation of the basic variable, and the sensitivity factor α_i of the variable.

Annex C of the Eurocode 0 provides expressions for the design values related to various distribution functions. Annex A of the current Eurocode 2 discusses an inspection-based reduction of partial factors, when the effective depth is measured on-site at an existing structure. This reduction of $\gamma_{S,red,2} = 1.05$ is however delimited by the German national annex. The national guideline for the reassessment of existing bridges allows a reduced partial factor of $\gamma_S = 1.05$ for the reinforcement steel if an additional surcharge $\Delta d_s = \pm 2$ cm is considered unfavorably in the effective depth. A reduced partial factor of

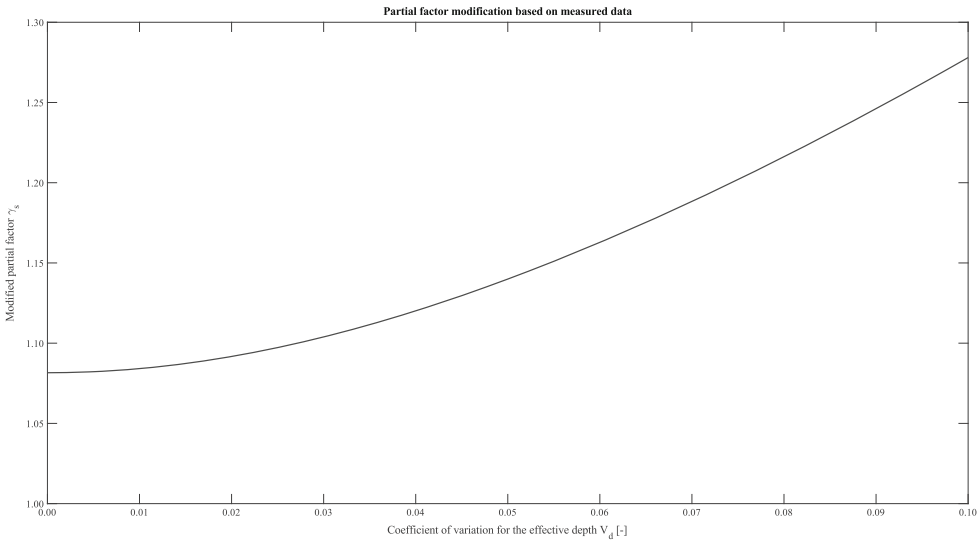

FIGURE 23 Modified partial factor over the coefficient of variation for the effective depth V_d.

$\gamma_S = 1.10$ is allowed for the prestressing steel if $\Delta d_s = \pm$ 1 cm is (again mathematically unfavorably) taken into account.

According to the fib bulletin and the model code 2010, the partial factor γ_M is obtained in general as the product $\gamma_M = \gamma_{Rd1} \cdot \gamma_{Rd2} \cdot \gamma_m$. For the partial factor of the reinforcement, the assumed values of $\gamma_{Rd1} = 1.025$ for the model uncertainties and $\gamma_{Rd2} = 1.05$ for the uncertainty of the reinforcement position are used. The fib bulletin 80 considers a coefficient of variation $V_x = 0.05$ for the reinforcement in new structure design, which leads (with $\alpha_R = 0.8$ and $\beta = 3.8$) to a partial factor $\gamma_m = (1 - 1.645 \cdot V_x)/(1 - \alpha_R \cdot \beta \cdot V_x) = 1.08$ accounting for the variability of the material and statistical uncertainties. The partial factor for the reinforcement then results in the well-known value of $\gamma_M = 1.025 \cdot 1.05 \cdot 1.08 \approx 1.15$.

The German national DBV-booklet 24 includes an approach, where the partial factor γ_M is calculated based on a coefficient of variation V_M that includes the model uncertainties. It must be noted, that the coefficient V_M is different from the coefficient of variation from statistical evaluation v_x. For a log. normal distributed function, the partial safety factor is given with $\gamma_M = \exp.(\alpha_R \cdot \beta \cdot V_M - k_R \cdot V_M)$. Assuming $\alpha_R = 0.8$; $\beta = 3.8$; $k_R = 1.645$ for a 5%-quantile and $V_M = 0.10$, this approach consistently yields $\gamma_M = \exp.(0.8 \cdot 3.8 \cdot 0.10 - 1.645 \cdot 0.10) = 1.15$.

The prEN 1992-1-1:2023 contains an approach with a single partial factor, where one coefficient of variation for the resistance V_{Rs} is used for the partial factor modification. V_{Rs} is based on the three coefficients of variations for (a) the yield strength $V_{fy} = 0.045$, (b) the effective depth $V_d = 0.050$ and (c) the model uncertainty $V_{\Theta s} = 0{,}045$, see Equation (7). Additional factors are given to cover systematical deviations: $\mu_d = 0.95$ and $\mu_{\Theta s} = 1.09$. As the yield strength is assumed to be log.-normally distributed and the characteristic value f_{yk} is a 5%-quantile, the term $f_{ym}/f_{yk} = \exp.(1.645 \cdot V_{fy})$ is used to describe the relation between the mean value f_{ym} and the characteristic value f_{yk}; see Equation (8). It must be noted that the values for V_d and μ_d are given for effective depths of 200 mm and need to be adjusted for other geometries. The partial factor γ_M again takes the value 1.15 as shown in Equation (9).

$$V_{RS} = \sqrt{V_{fy}^2 + V_d^2 + V_{\Theta s}^2} = \sqrt{0.045 + 0.050 + 0.045} = 0.081 \tag{7}$$

$$\mu_{RS} = \exp\left(1.645 \cdot V_{fy}\right) \cdot \mu_d \cdot \mu_{\Theta s} = 1.077 \cdot 0.95 \cdot 1.09 = 1.115 \tag{8}$$

$$\gamma_M = \frac{\exp\left(\alpha_R \cdot \beta_{target} \cdot V_{RS}\right)}{\mu_{RS}} = \frac{\exp(0.8 \cdot 3.8 \cdot 0.08)}{1.115} \approx 1.15 \tag{9}$$

Since additional information about the position of the tendons were gained in this pilot study through on-site NDT, the partial factor can be adjusted based on $V_{d,NDT} = 7.5$ mm/241 mm $= 0.031$ using Figure 23.

3.4 | Summary of results and interpretation

The results of the three reliability analysis phases are summarized in Table 4. In semi-probabilistic assessment, the utilization degree in the different cross-sections varies between 9% and 78% (see Figures 12 and 13). For the in-depth investigated slab section S3, a percentage of 48% has been initially observed. The utilization increases in the probabilistic analysis slightly by 7% (or decreases

TABLE 4 Comparison of utilization degrees observed in the three reliability assessment stages.

Reliability assessment	Numerical reliability	Target reliability	Utilization degree
Semi-probabilistic w/o NDT	Ratio ultimate/numerical moment = 2.07		48%
FORM w/o NDT	$\beta = 6.90$	$\beta_t = 3.8$ ($\beta_t = 3.1$ for existing structures[52])	55% (45%)
SORM w/o NDT	$\beta = 6.87$		55% (45%)
FORM w/NDT	$\beta = 6.88$		55% (45%)
SORM w/NDT	$\beta = 6.85$		55% (45%)

marginally by 3% when comparing to target beta for existing structures). The explicit consideration of the on-site NDT results, in this case about the transversal tendon position, yields no significant changes in reliability. Although the uncertainty initially attributed to this geometrical dimension could be reduced from $\sigma_{w/o,-NDT} = 10$ mm to $\sigma_{w/,NDT} = 7.5$ mm, the slight but numerically unfavorable deviation between the measured ($\mu = 241$ mm) and planned ($\mu = 245$ mm) position equalizes the effects on the computed reliability index. Overall, the measured information in this individual case is consistent with the previously available drawings.

The relevant and nondestructively measurable geometrical basic variables in this ULS bending analysis have been found to be the inner lever arm and the vertical position of the transversal tendons. Sound knowledge about the mean increases the validity of the computation results, while an uncertainty reduction influences reliability noticeably, i. a. due to the thinness of the slab. It would be further desirable to establish a measurement technique to determine the prestressing steel strength. An example for a qualitative inspection objective that is relevant for this proof is the corrosion state of the anchor heads, which could be determined using radiographic testing depending on the used equipment and component thickness.

4 | CONCLUSION AND OUTLOOK

A reassessment yields valuable insights about the reliability of an existing structure, which are needed to extend its service life as well as to make better decisions about actions to be taken and future maintenance strategies. The application requires various information about the considered system. The presented research activities aim to demonstrate the potentials of supporting the reliability assessment through on-site NDT. Main findings of this case study are:

- The sole assessment of an existing bridge based on absolute probabilistic analysis results might lead to biased decisions as i. a. the irregulated stochastic modeling process causes lacks in comparability.
- A number of input quantities relevant in reliability assessment according to the Eurocodes are nondestructively measurable. Depending on the measured value, the reduction of uncertainties does not necessarily result in higher computational reliability.
- On-site measurements are particularly useful when information is incomplete or in doubt. Inspection-based updates might be useful to confirm utilization degrees close to thresholds.
- Structural clarification through NDT is particularly efficient for component thicknesses and steel contents that are not too great. Needs for metrological developments exist, e.g., with regard to the determination of prestressing forces and investigation of grouting conditions.

The activities aim to propose a procedure that can be applied efficiently in practice to modify partial factors structure-specifically and to incorporate characteristic values based on performed on-site NDT. In this way, it is intended to spare the engineer the detours via probabilistic analysis and time-consuming modeling during measurement uncertainty calculations when utilizing NDT results in reassessment. The project results are expected to be published in 2025.

ACKNOWLEDGMENTS

The authors gratefully acknowledge the financial support of the *German Federal Ministry for Economic Affairs and Climate Action* under grant number 03TN0042, the approval by the *building authority Freising* to inspect the structure as part of the research activities and the support on-site by *A. Schimkus* and *P. Lieberwirth* (HTW Berlin). Open Access funding enabled and organized by Projekt DEAL.

DATA AVAILABILITY STATEMENT

The data that support the findings of this study are available from the corresponding author upon reasonable request.

ORCID

Stefan Küttenbaum https://orcid.org/0000-0003-2603-0032
Christian Kainz https://orcid.org/0009-0005-5482-4923

REFERENCES

1. Bundesanstalt für Straßenwesen: Brückenstatistik. Stand: 01.09.2023. [cited 2024 Apr 1]. Available at: https://www.bast.de/DE/Statistik/Bruecken/Brueckenstatistik.pdf
2. Bundesanstalt für Straßenwesen: Brückenstatistik. Excel-File. [cited 2024 Apr 1]. Available at: https://www.bast.de/DE/Ingenieurbau/Fachthemen/brueckenstatistik/bruecken_hidden_node.html
3. Richtlinie zur Nachrechnung von Straßenbrücken im Bestand (Nachrechnungsrichtlinie), 05/2011 [in German].
4. Nachrechnungsrichtlinie, 1. Ergänzung, 04/2015 [in German].
5. DIN 1076:2024-02 – Draft. Engineering structures in connection with roads – Inspection and test. [in German] https://doi.org/10.31030/3510975
6. Fischer O, Müller A, Lechner T, Wild M, Kessner K. Ergebnisse und Erkenntnisse zu durchgeführten Nachrechnungen von Betonbrücken in Deutschland. Beton-und Stahlbetonbau. 2014;109:107–27. [in German].
7. Maurer R, Zilch K, Dunkelberg D, Kolodziejczyk A. Effektive Steifigkeiten, Anrechenbarkeit von Spanngliedern und heute unzulässige Bewehrungsformen beim Nachweis für Querkraft- und Torsion bei Bestandsbrücken. Bauingenieur. 2014;98:511–20.
8. Hegger J, Mauer R, Zilch K, Herbrand M, Kolodziejczyk A, Dunkelberg D. Beurteilung der Querkrafttragfähigkeit des Längssystems von Spannbetonbrücken im Bestand. Bauingenieur. 2014;89:500–10.
9. Hegger J, Fischer O, Maurer R, Dommes C, Adam V, Lamatsch S, et al. Querkraft und Torsion – zukünftige Ansätze und Potenziale in Stufe 2 der Nachrechnungsrichtlinie. Bauingenieur. 2024;99:1–11. [in German].
10. Hegger J, Fischer O, Maurer R, Zilch K, Dommes C, Adam V, et al. Nachrechnungen von Spannbetonbrücken mit Verfahren der Nachrechnungsstufe 4. Bauingenieur. 2024;99:12–21.
11. fib Bulletin 109. Existing concrete structures life management, testing and structural health monitoring. State-of-the-art-report (151 pages, ISBN 978-2-88394-172-4). 2003.
12. fib Bulletin 22. Monitoring and safety evaluation of existing concrete structures. State-of-art report (304 pages, ISBN 978-2-88394-062-8). 2003.
13. Fischer J, Straub D, Schneider R, Thöns S, Rücker W. Intelligente Brücke—zuverlässigkeitsbasierte Bewertung von Brückenbauwerken unter Berücksichtigung von Inspektions und Überwachungsergebnissen. Berichte der BaSt: Heft B 99. Fachverlag NW: Bremen; 2014.
14. EUR 22906 EN. ENIQ report no. 31. Third ed. 2007.
15. Küttenbaum S, Braml T, Taffe A, Keßler S, Maack S. Reliability assessment of existing structures using results of nondestructive testing. Struct Concr. 2021;22:2895–915. https://doi.org/10.1002/suco.202100226
16. fib Bulletin 80. Partial factor methods for existing concrete structures. Recommendation (129 pages, ISBN 978-2-88394-120-5) 2016.
17. Hasofer AM, Lind NC. Exact and invariant second-moment code format. J Eng Mech Div. 1974;100:111–21.
18. Rackwitz R, Fiessler B. Structural reliability under combined random load sequences. Comput Struct. 1978;9:489–94. https://doi.org/10.1016/0045-7949(78)90046-9
19. Hohenbichler M, Rackwitz R. Non-normal dependent vectors in structural safety. J Eng Mech Div. 1981;107:1227–38.
20. DGZfP-B-LF 01. 2022–04 Leitfaden zur Erstellung von Prüfanweisungen für die Zerstörungsfreie Prüfung im Bauwesen (ZfP Bau). [in German].
21. Küttenbaum S, Maack S, Aßmann N, Feistkorn S. Ways to unlock the potential of non-destructive concrete testing for the reliability assessment of our built environment. Proc. SPIE 12491, 8th international workshop on reliability of NDT/NDE, 1249107. 2023 https://doi.org/10.1117/12.2658736
22. Küttenbaum S, Feistkorn S, Braml T, Taffe A, Maack S. Methods to quantify the utility of NDT in bridge reassessment. In: von Rizzo P, Milazzo A, editors. European workshop on structural health monitoring: special collection of 2020 papers. New York: Springer; 2021. p. 403–13.
23. JCGM 100:2008 (GUM 1995 with minor corrections). Evaluation of measurement data – Guide to the expression of uncertainty in measurement.
24. Taffe A. Zur Validierung quantitativer zerstörungsfreier Prüfverfahren im Stahlbetonbau am Beispiel der Laufzeitmessung. DAfStb-Heft. 2008;574:828–36.
25. Küttenbaum S. Zur Validierung von zerstörungsfreien Messverfahren für die probabilistische Beurteilung von Bestandsbauwerken mit gemessenen Daten. Dissertation, München. 2021.
26. JCSS Probabilistic Model Code Part 1–3. Zurich: Joint Committee on Structural Safety; 2001-2002.
27. Kiureghian AD, Ditlevsen O. Aleatory or epistemic? Does it matter? Struct Saf. 2009;31(2):105–12. https://doi.org/10.1016/j.strusafe.2008.06.020
28. Diamantidis D. Probabilistic assessment of existing structures: a publication of the joint committee on structural safety (JCSS). Cachan: RILEM Publications; 2001.
29. Küttenbaum S, Maack S, Taffe A, Braml T. On the treatment of measurement uncertainty in stochastic modeling of basic variables. Acta Polytechnica CTU Proceedings. 2022;36:109–18.
30. Braml T. Zur Beurteilung der Zuverlässigkeit von Massivbrücken auf der Grundlage der Ergebnisse von Überprüfungen am Bauwerk, Univ. d. Bundeswehr München, Diss. 2010.
31. Fischer AM. Bestimmung modifizierter Teilsicherheitsbeiwerte zur semiprobabilistischen Bemessung von Stahlbetonkonstruktionen im Bestand TU Kaiserslautern, Diss. 2010.
32. Özlü C, Küttenbaum S, Kainz C, Braml T, Taffe A. Probabilistischer Nachweis einer Spannbetonbrücke – Teil 2. Beton- und Stahlbetonbau. 2024;119(9):622–635.
33. DIN 4871:2022–09. Non-destructive testing – Qualification of NDT personnel in Civil Engineering (NDT-CE).
34. fib Bulletin 22. Monitoring and safety evaluation of existing concrete structures. State-of-art report (304 pages, ISBN 978-2-88394-062-8) 2003.
35. Küttenbaum S, Braml T, Heinze M, Kainz C, Keuser M, Kotz P, et al. Guideline on NDT-supported reliability assessment of existing structures – current developments in Germany. Ce/papers. 2023;6(5):537–43.
36. DIN 1072:1985-12/withdrawn. Road and foot bridges; design loads. [in German].
37. DIN-Fachbericht 101:2009-03/withdrawn. Actions on bridges. [in German].
38. DIN-Fachbericht 102:2009-03/withdrawn. Concrete bridges. [in German].
39. Strurel. RCP consult GmbH. Munich, Germany: Strurel; 2024.
40. Kainz C, Braml T, Keuser M, Soukup A, Küttenbaum S. Reassessment of existing concrete bridges with full probabilistic methods – case studies and discussion of relevant input

parameters. 2024. In: Proceedings of the 20th International Probabilistic Workshop. ISBN 978-3-031-60271-9.
41. Fischer AM. Bestimmung modifizierter Teilsicherheitsbeiwerte zur semiprobabilistischen Bemessung von Stahlbetonkonstruktionen im Bestand, Dissertation. 2010 Technische Universität Kaiserslautern, Kaiserslautern.
42. Vejdirectoratet. Reliability-based classification of the load carrying capacity of existing bridges – report 291. Road Directorate, Ministry of Transport, Denmark. 2004.
43. Müller HS, Acosta Urrea F, Kvitsel V. Modelle zur Vorhersage des Schwindens und Kriechens von Beton –Teil 2b: Kriechen –Neuer Ansatz im Eurocode 2prEN 1992-1-1:2021. Beton- und Stahlbetonbau. 2021;116:806–20. https://doi.org/10.1002/best.202100084
44. Steffens N. Sicherheitsäquivalente Bewertung von Brücken durch Bauwerksmonitoring [Dissertation]. 2019 Technische Universität Berlin.
45. Kainz C, Lapidus L, Braml T. Modelling of traffic loads in a full-probabilistic reassessment of rural bridges based on measurement data – a case study. 2024. 20th international probabilistic workshop. https://doi.org/10.1007/978-3-031-60271-9_17
46. Bach T. Tragfähigkeitsnachweise von Stahlbetonquerschnitten bei Biegebeanspru-chung mit und ohne Längskraft auf der Grundlage der Zuverlässigkeitstheorie der Stufe II [Dissertation]. 1992 Technische Universität Dresden.
47. JCSS. Probabilistic Model Code. Part 1-3. Zürich: Joint Committee on Structural Safety; 2001/2002.
48. Jacinto L, Pipa M, Neves LA, Santos LO. Probabilistic models for mechanical properties of prestressing strands. Constr Build Mater. 2012;36:84–9.
49. JCGM 100:2008. Evaluation of measurement data – Guide to the expression of uncertainty in measurement.
50. Taffe A. DAfStb-Heft 574. Zur Validierung quantitativer zerstörungsfreier Prüfverfahren im Stahlbetonbau am Beispiel der Laufzeitmessung. Berlin: Beuth; 2008.
51. Küttenbaum S, Maack S, Taffe A. Approach to the development of a model to quantify the quality of tendon localization in concrete using ultrasound. MATEC Web Conf. 2022;364:03007. https://doi.org/10.1051/matecconf/202236403007
52. Federation international du béton (fib). Fib bulletin 80 – partial factor methods for existing concrete structures. Recommendation, fib task group 3.1. 2016.
53. fib Model Code for Concrete Structures 2020 (MC2020), ISBN 978-2-88394-175-5 2023.
54. Deutscher Beton- und Bautechnik Verein. DBV Heft 24 – Begründung eines reduzierten Zuverlässigkeitsindexes und modifizierter Teilsicherheitsbeiwerte für Stahlbetontragwerke im Bestand. 2014.

AUTHOR BIOGRAPHIES

Dr.-Ing. Stefan Küttenbaum Universität der Bundeswehr München, Department of Structural Engineering, Werner-Heisenberg-Weg 39, 85577 Neubiberg (Germany), stefan.kuettenbaum@unibw.de

Prof. Dr.-Ing. Thomas Braml, Universität der Bundeswehr München, Department of Structural Engineering, Werner-Heisenberg-Weg 39, 85577 Neubiberg (Germany). thomas.braml@unibw.de

Dipl.-Ing., Dipl.-Wirtsch.-Ing. Marco Heinze, ZM-I München GmbH, Erika-Mann-Straße 63, 80636 Munich (Germany), marco.heinze@zm-i.de

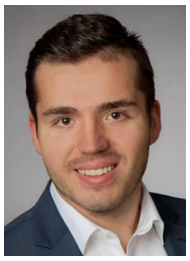

Dipl.-Ing. Christian Kainz, Universität der Bundeswehr München, Department of Structural Engineering, Werner-Heisenberg-Weg 39, 85577 Neubiberg (Germany), christian.kainz@unibw.de

Dr.-Ing. Christian Stettner, ZM-I München GmbH, Erika-Mann-Straße 63, 80636 Munich (Germany), christian.stettner@zm-i.de

Prof. Dr.-Ing. Alexander Taffe, HTW Berlin – University of Applied Sciences, Department 2: Engineering – Technology and Life, Wilhelminenhofstraße 75a, 12459 Berlin (Germany), alexander.taffe@htw-berlin.de

How to cite this article: Küttenbaum S, Braml T, Heinze M, Kainz C, Stettner C, Taffe A. Reliability and partial factor-based assessment of a highway bridge supported by nondestructive testing. Structural Concrete. 2025;26(5):5535–54. https://doi.org/10.1002/suco.202400717